Macromolecules

ARTICLE

pubs.acs.org/Macromolecules

Extension Flow Induced Crystallization of Poly(ethylene oxide)

Nan Tian, Weiqing Zhou, Kunpeng Cui, Yanping Liu, Yuye Fang, Xiao Wang, Liangbao Liu, and Liangbin Li*

National Synchrotron Radiation Lab and College of Nuclear Science and Technology, CAS Key Laboratory of Soft Matter Chemistry, University of Science and Technology of China, Hefei, China

ABSTRACT: Crystallization of poly(ethylene oxide) (PEO) induced by extensional flow has been studied by in-situ small-angle X-ray scattering (SAXS). A constant Hencky strain was applied to the melt with strain rates varying in 3 orders of magnitude. The evolution of the long period with crystallization time is qualitatively different for high and low strain rates. In the region of high strain rates the long period first increases, reaches a plateau, and decreases in the later stage of crystallization. In contrast, for low strain rates only a monotonic decrease is observed. Given the high orientation in the high strain rate region, we propose a localized nucleation mechanism (like row-nuclei). The initial increase of the long period for high strain rates indicates a decrease of nucleation density, which is the inverse of the long period. On the basis of the microrheological model proposed by Coppola et al., in which the flow induced free energy change under steady state flow is calculated with the Doi−Edwards model, we develop a framework describing the nucleation after a step strain with high strain rates. By introducing the memory function, the dynamic process of relaxation is taken into account, leading to a continuous decrease of the nucleation density. Numerical fitting the model to the experimental data gives a good agreement with the terminal relaxation time τ_d, the volume filling rate B, and a constant C_3 determined by surface free energy of the nuclei as fitting parameters. The results confirm the localized nucleation mechanism in highly oriented melt. Furthermore, the fitted value of C_3 indicates a drop in surface free energy of nuclei under strong flow.

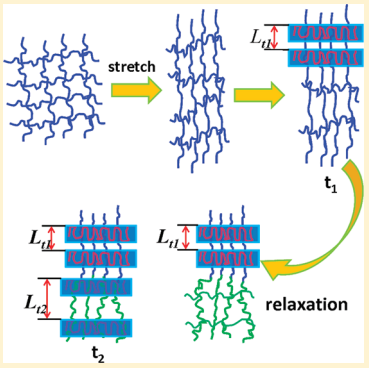

INTRODUCTION

During processing polymer melts are generally subjected to different types of flow field. Flow field affects crystallization of polymer through inducing orientation and stretch of chain, whose effects show up in different ways such as accelerating crystallization kinetics,[1,2] modifying the morphology from spherulite to shish-kebab,[3,4] and inducing new crystal forms.[5,6] Consequently, the final performance of the resulting product depends strongly on the flow field during processing. Flow induced crystallization (FIC) is considered to be a promising approach for tuning the properties of polymer products, which has been extensively studied in the past decades.

As almost all effects of flow on crystallization are directly related to nucleation, flow induced nucleation is the focus in studies of FIC. Nevertheless, due to its complexity, contradictory views have been reported regarding several fundamental issues. These include the initial response of the chain under flow, effects of possible preordering, models for nuclei, and the role of molecular and external field parameters. A brief summary of these issues will be given here. (I) The first point regards the occurrence of coil−stretch transition (CST) of a single chain or a stretched network upon imposing a strong flow. Since the first observation of Pennings[7] and Keller,[8] this has been a matter of debate. Pioneer work by Keller et al.[9,10] on dilute and semidilute solution indicates an abrupt CST in extensional flow. This idea has been extended to the interpretation of shish formation in the polymer melt. In the latter any flow induced stretch is expected to relate to the transient network of entanglement. Recent rheo-SAXS experiment excludes CST of the whole chain.[11] Nevertheless, the idea of CST may be still valid at the level of segments[3] though the CST is already different from its initial definition. (II) The next question is whether preordering is a necessary step in nucleation. Classical crystallization theory assumes an abrupt transition from melt to nuclei, while increasing evidence has become available pointing to the existence of an intermediate state, generally referred to as preordering or precursor. These results include flow induced conformational ordering,[12,13] the existence of a memory effect,[14−16] spinodal decomposition,[17−21] and evidence from computer simulations.[22] Though in-situ small- and wide-angle X-ray scattering experiments give some evidence,[23−27] it is still disputed. The existence of preordering seems to be widely accepted now; questions regarding the structure of the preordering and its transformation to nuclei are left. (III) The next point is the correct description of the structure of nuclei. Can the folded-chain model or better the fringed-micelle model be used? The low end surface free energy of folded-chain model, corresponding to a low nucleation barrier, has been used to exclude fringed-micelle model in quiescent nucleation, which has been reiterated with the presence of preordering or entropy consideration.[28−30] However, in the presence of strong flow, a polymer melt will be highly oriented and stretched. The extra barrier in fringed-micelle model, which originates in entropy loss, then could be overcome by the flow. The initial concept of a shish with a structure of extended-chain

Received: June 4, 2011
Revised: August 24, 2011
Published: September 13, 2011

crystal matches in this limit well with the fringed-micelle model. The correlation between an isolated single nucleus, a series of line nuclei, and shish still has to be determined. (IV) Whether long chains dominate in flow induced nucleation or synergy of long and short chains is essential? In line with the early CST concept of shish formation, long chains relax slowly and the residual orientation leads to a lower nucleation barrier, a higher thermodynamic driving force, and a faster nucleation rate. This seems to be largely confirmed by various experiments.[31−34] However, the difficulty to control molecular parameters of long and short chain in experiments makes unambiguous evidence scarce to be found. Recent evidence suggests that synergy between the effects of long chains on the nucleation barrier and of short chains on fast diffusion may be decisive for accelerating nucleation.[35−37] (V) It is difficult to link flow parameters to the deformation of chains. In a FIC experiment apparent parameters are set, and the resulting crystallization is monitored. However, the actual deformation of chains is unknown. Shear flow, which is commonly used in FIC experiment, can be inhomogeneous.[38−42] Moreover, molecular relaxation plays an important role in nucleation during and after flow.[42] All these factors make it difficult to link the apparent flow parameters directly to chain deformation.

Incorporating external work quantitatively into the free energy of molecular chains is a first step to establish a thermodynamic model of flow induced nucleation. This remains a challenge even without taking conformational order and other preordering with enthalpy change into account. Restricting entropic loss to the chain orientation and stretch is still problematic due to the complication of inhomogeneous flow and a rudimentary state of theory of nonlinear chain dynamics. Phenomenologically, a link can be constructed between crystallization kinetics and flow field. In the modified Nakamura's approach[43] flow parameters such as strain,[44] strain rate,[45] and stress[46] are linked to factors in the crystallization kinetic function. This approach provides an empirical relation between flow parameters and crystallization kinetics but without any molecular information. Correlating external work from flow with crystal orientation shows a critical specific work is required to form oriented nuclei when the strain rate is higher than the inverse of the Rouse time of long chains.[47,48] More general, but also more complicated, descriptions based on continuum theory[49−51] have been widely used to relate the elasticity of the melt and the energy stored in chain. In this way parameters reflecting the stress and strain state of the melt can be related to the driving force of flow induced nucleation. This approach gives more information on the crystallization process, such as nucleation density and half-time of crystallization.

A molecular theory would involve chain dynamics and a specific nucleation model. An attempt has been made using the dumbbell model[52−54] and the Doi−Edwards model. The microrheological model based on the Doi−Edwards model incorporating independent alignment approximation (IAA) seems promising to predict the enhancement of crystallization kinetics for a large range of strain rate.[55,56] The introduction of the memory function clearly declares the effect of relaxation in FIC and makes quantitative prediction possible. The model, however, so far analyses only steady-state flow. The dynamic character of relaxation and the corresponding nucleation after flow, generally faced in the step-strain experiments, is not embodied. Thus, a more comprehensive analysis is required to cover the whole nucleation process in FIC.

In this work, a combination of extensional rheology and in-situ synchrotron radiation SAXS measurements has been used to investigate flow induced nucleation of PEO. The emphasis is on the correlation between strain rate and nucleation rate. The evolution of the long period during crystallization shows different trends at high and low strain rates. An extension on the original microrheological model is developed to describe the nucleation after a step strain with high strain rates. A good agreement between our experimental results and theoretical calculation is obtained.

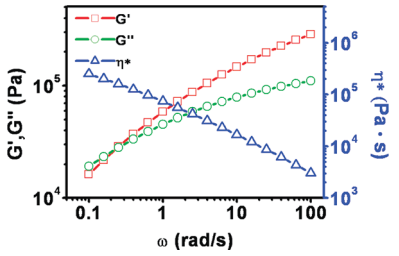

Figure 1. Result of SAOS measurement at 100 °C.

EXPERIMENT

PEO was used in this work for a relatively narrow molecular weight distribution compared to commercial polyethylene and polypropylene, which is important for modeling on molecular level. The sample was purchased from Lian Sheng Chemical Co. of Shanghai. The molecular weight distribution was determined by gel permeation chromatography using a Waters 1515 isocratic HPLC pump and water as solvent. The weight-average molecular weight (M_w) was 1070 kg/mol, and the polydispersity index was 1.4. The melting point was determined to be 66.2 °C by differential scanning calorimetry (DSCQ2000, TA Instruments) at a heating rate of 10 °C/min. The terminal relaxation time τ_d was determined by small-amplitude oscillation shear (SAOS), using the rheometer AR2000EX equipped with parallel plates with a diameter of 25 mm. The result was 4 s at 100 °C (see Figure 1) and 10 s at 90 °C. PEO powder was dried under vacuum at 55 °C for 12 h and then molded to a plate with a thickness of 1 mm by a vulcanizing press at 80 °C. The samples to be studied were cut into rectangular shape with dimensions of 30 × 20 × 1 mm^3.

A schematic picture of the homemade two-drum extensional rheometer used in this work is shown in Figure 2. Its design is similar to the Sentmanat extensional rheometer, and Hencky strain can be obtained. The sample was secured on two geared drums by means of clamps. Subsequently, stretching was carried out through the rotation of motor, which drives the geared drums rotating in opposite directions. The torque is measured through the torque sensor connecting the drums and the motor. Note with strain rates higher than 50 s^{-1} the motor start gives a shock on torque sensor, which reduces the accuracy of torque measurements. The basic formula used is $\dot{\varepsilon} = 2v/l_0$, in which $\dot{\varepsilon}$ is the Hencky strain rate, v the linear velocity at the surface of the drum, and l_0 the length of sample being stretched (equal to the axes distance of the drums). As l_0 is kept constant during stretching, different values of strain rate can be obtained by varying v.

Each sample was first heated to 80 °C and held for 10 min to erase thermal history. Then it was cooled to the crystallization temperature of 58 °C with a rate of 2 °C/min. A nitrogen gas flow helped to homogenize the temperature and prevent sample degradation. The temperature fluctuations were within ±0.5 °C. The extension by a step strain was imposed on the supercooled melt immediately after reaching 58 °C. The Hencky strain ε was kept as constant at 1.2, while strain rate was varied from 0.1 to 100 s^{-1} (3 orders). Immediately after the cessation of extension, the crystallization was monitored by in-situ SAXS measurements at the beamline BL16B1 of Shanghai Synchrotron Radiation

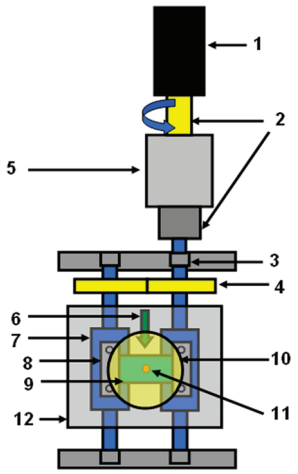

Figure 2. Schematic drawing of the extensional rheometer for in-situ SAXS measurements: 1, the servo motor; 2, the coupler; 3, bearings; 4, gears; 5, The torque sensor; 6, the nitrogen gas flow; 7, drums; 8, clamps fixed with screw; 9, sample; 10, the scattering window covered by Kapton film; 11, the detection point at the middle of the sample; 12, the heating oven.

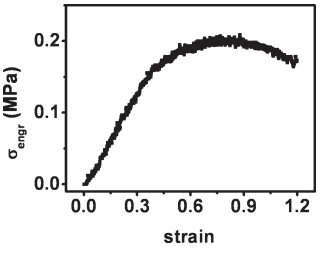

Figure 3. Engineering stress−strain curve at a strain rate of 1 s^{-1}.

Facility. The X-ray wavelength was 0.154 nm, and a Mar165 CCD detector (2048 × 2048 pixels with pixel size 80 μm) was employed to collect time-resolved two-dimensional (2D) SAXS patterns. The sample-to-detector distance was 5145 mm. Fit2D software from European Synchrotron Radiation Facility was used to analyze SAXS patterns in term of the scattering vector $q = 4\pi \sin \theta/\lambda$ with 2θ as the scattering angle and λ as the X-ray wavelength. Lorentz correction was applied to all the one-dimensional intensity profile.

EXPERIMENTAL RESULTS

FIC experiments with extensional rheo-SAXS measurements have been conducted with nine different strain rates from 0.1 to 100 s^{-1}. The crystallization behaviors fall in two groups: high and low strain rates. Figures 3 and 4 give the results for a strain rate of 1 s^{-1}, typical for low strain rates. The engineering stress−strain curve during the step strain is presented in Figure 3. Initially, the stress increases almost linearly with strain. After passing the linear viscoelastic region, the increase of stress with strain slows down, leading to a stress maximum at a strain of 0.8. After cessation of the step strain, it takes a relative long time before crystallization starts. Several representative 2D SAXS patterns are presented in Figure 4a. At the onset of crystallization, the 2D SAXS patterns show an elliptic isointensity contour with its long axis paralleling to the extensional direction. Increasing the crystallization time the elliptic SAXS pattern transforms into a spindle shape. Finally, a clear scattering maximum due to the

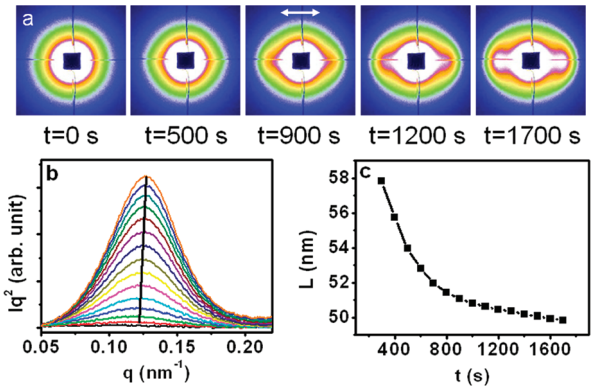

Figure 4. (a) 2D SAXS patterns of PEO after being stretched with a strain and strain rate of 1.2 and 1 s^{-1}, respectively. The arrow indicates the extensional direction. (b) 1D SAXS intensity profiles. (c) Evolution of the long period during the crystallization process.

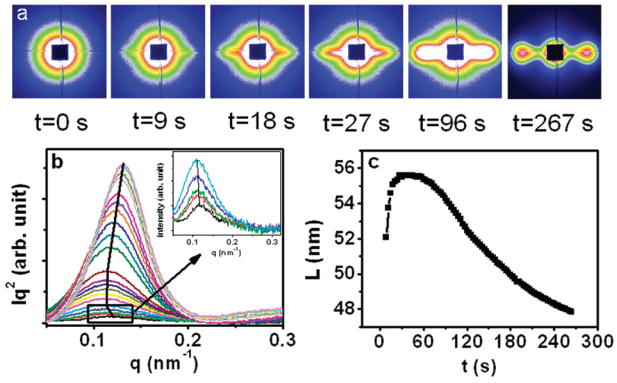

Figure 5. (a) 2D SAXS patterns of PEO after being stretched with a strain and strain rate of 1.2 and 100 s^{-1}, respectively. (b) 1D SAXS intensity profiles. (c) Evolution of long period during crystallization process.

periodicity of lamellar crystals emerges, which is shifting gradually to the large-q side. One-dimensional (1D) SAXS intensity profiles during crystallization are shown in Figure 4b, in which the shift of the peak position is highlighted with a tilted line. The evolution of the long period (L) during crystallization is shown in Figure 4c. L is about 58 nm at the onset of crystallization and shows a monotonic decrease reaching a plateau of about 50 nm at the end of crystallization.

For high strain rates 100 s^{-1} is selected as the representative. The stress−strain curve is not given here for the low reliability, which comes from an increased influence of the motor start on the accuracy of torque measurement. The SAXS results are presented in Figure 5. Similar as for low strain rates, a quick evolution from elliptic to spindle shapes is observed, which eventually results into meridional streaks in the extensional direction. Increasing the crystallization time, the streaks become stronger and extend to larger q. Though the scattering streaks in the extensional direction are rather similar to those from shish, they can be explained either by Hsiao's lamellae model[34] with wide distributions of periodicity and lateral size or Stribeck's block model.[57] 1D SAXS intensity profiles are shown in Figure 5b, where the intensity profiles at the beginning of crystallization is enlarged as an inset. The scattering maximum

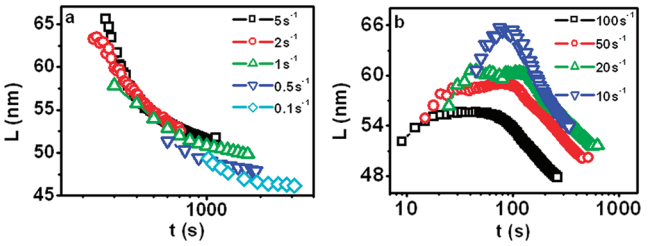

Figure 6. Time evolution of the long period. (a) Low strain rate region including 0.1, 0.5, 1, 2, and 5 s^{-1}. (b) High strain rate region including 10, 20, 50, and 100 s^{-1}.

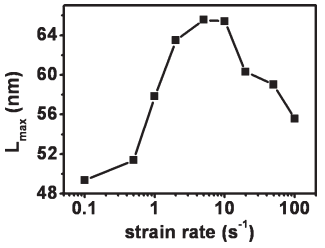

Figure 7. Maximum value of the long period vs strain rate.

shifts first to low-q side and then back to large-q direction, different from the situation for low strain rates. The evolution of L follows a nonmonotonic process during crystallization as presented in Figure 5c. In the early stage, the long period increases from about 52 nm to a plateau level of about 56 nm. At crystallization time of about 60 s, L decreases again and reaches about 48 nm at the end of the experiment. The later behavior is similar to that at low strain rates (see Figure 4c).

The effect of strain rate has been studied for seven other strain rates. Figures 6a and 6b present the evolutions of long period during crystallization after subjected to step strains with low and high strain rates, respectively. The transition between the evolution of L for low and high strain rates occurs between 5 and 10 s^{-1} (see Figure 6). The rapid decreasing part of L has been attributed to insertion of new lamellar into existing lamellar stacks as also observed during crystallization of PEO at quiescent conditions.[58] With strain rates larger than 10 s^{-1}, the initial rapid increase of long period appears and the decrease of L occurs at a later stage.

The maximum value of L is plotted in Figure 7 as a function of strain rate. The trend is again nonmonotonic, similar to the nonmonotonic evolution of L with crystallization time in high strain rate region. Evidently, in this region two competitive mechanisms govern the periodicity of the lamellar crystals. The first mechanism is insertion of new lamellar crystals in the initially formed stacks. This mechanism should work in both high and low strain rate regions and governs the decreasing part of the variation of L. The second mechanism is responsible for the increase of L in the high strain rate region, which dominates the evolution of L at early stage or the nucleation stage. The initial increase of L is attributed to decreased nucleation density related to the relaxation of polymer chain. This will be discussed later in more detail using the extension of the microrheological model proposed by Coppola et al.

The orientation of lamellar crystals in the final crystallized samples can be characterized by Herman's orientation parameter

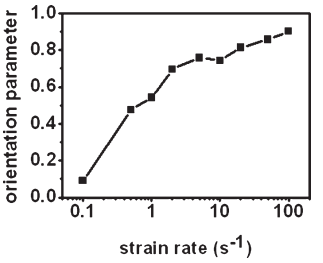

Figure 8. Orientation parameter vs strain rate.

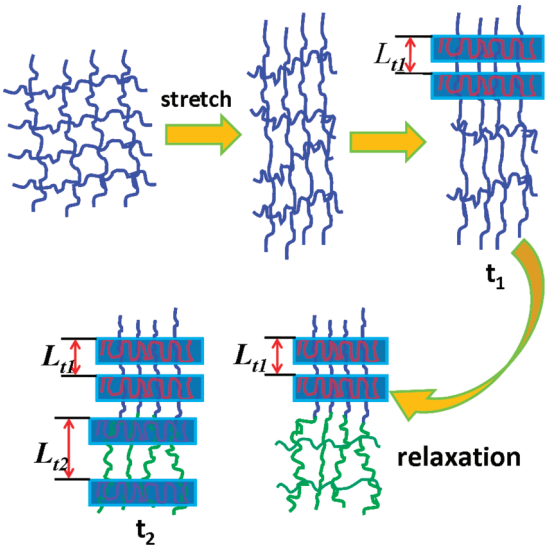

Figure 9. Schematic illustration of the nucleation model after a step strain. The nucleation density decreases (long period increases) with nucleation time due to the relaxation of polymer chains.

f, which is defined as

$$f = \frac{3\langle \cos \varphi^2 \rangle - 1}{2} \quad (1)$$

Here φ is the angle between the reference direction (extensional direction) and the normal direction of the lamellae. Thus, f has a value of 1 when all lamellae are perpendicular to the flow direction, a value of 0 when the lamellae have no preferred orientation, and a value of −0.5 when all lamellae are parallel to flow direction. The result is presented in Figure 8. The orientation increase with strain rate but there is a small anomaly in the trend around a strain rate of 5 s^{-1}. Below 5 s^{-1} the orientation increases sharply with strain rate, while above 10 s^{-1} the strain rate leads to slower increase of the orientation parameter. Evidently this transition coincides with the limits of high and low strain rate regions as observed from the evolution of L.

THEORETICAL MODELING

In order to explain the increase of long period in the early stage of crystallization after subjected to a step strain with high strain rates, we develop a theoretical model to capture the dynamic character of nucleation after a step strain. A schematic illustration of the model is presented in Figure 9. After the cessation of the step strain at time t_0, the highly oriented molecular chains go

dx.doi.org/10.1021/ma201263z |Macromolecules 2011, 44, 7704–7712

through a continuous relaxation process back to their equilibrium state, during which flow induced nucleation takes place. No enthalpy change (e.g., preordering) but only entropy loss is considered here for simplification. The influence of orientation on the growth kinetics is also not considered for no rigorous evidence has been proposed. In the situation of high orientation, nucleation is localized, as in the situation of row-nuclei or shish-kebab. Thus, the long period is proportional to the inverse of linear density of nuclei. Evidently, the nuclei density decreases with time due to the relaxation of the oriented polymer network or dispersing of free energy provided by the step strain, which can be characterized with the so-called memory function. Correspondingly, the long period increases with nucleation time, namely $L_{t_1} < L_{t_2}$ with $t_1 < t_2$ as schematically illustrated in Figure 9. The long period obtained with SAXS is the inverse of the nucleation density averaged over total nucleation time, which also increases with time.

With the model in mind the long period can be predicted by eq 2 if the nucleus number $N(t)$ and the occupied one-dimensional volume $V(t)$ are known.

$$L(t) \sim \frac{V(t)}{N(t)} \tag{2}$$

The microrheological model of Coppola et al. calculated the entropy loss induced by flow using the Doi−Edwards theory with independent alignment approximation, which has been proven to predict the rheological behavior of polymer melts in a quite reasonable (although not perfect) way. Though some specifics of the chain are neglected compared to computer simulation,[59,60] the model can give an analytical and relatively simple expression. In the following section, we will extend the microrheological theory to interpret the evolution of long period during the nucleation stage quantitatively. First, we will give the expression of nucleation rate of unit volume after cessation of the step strain. The deduction of original microrheological model for arbitrary deformation history is given first, and then a modification to include step strain is proposed. Subsequently, the volume occupied by nuclei is derived with the assumption that the volume filling rate B is constant. Finally, combining the nucleation rate and the filling rate, we obtain the expression of the time dependent long period, which will be used to compare with our SAXS results.

I. Calculation of Nucleation Rate of Unit Volume. Let us first recall the microrheological model proposed by Coppola et al. According to the theory of Lauritzen and Hoffman,[61,62] the nucleation rate can be expressed as

$$\dot{N} = Ck_BT\Delta G \exp\left(-\frac{E_a}{k_BT}\right) \exp\left[-\frac{K_n}{T(\Delta G)^n}\right] \tag{3}$$

where C includes energetic and geometrical constant, k_B is the Boltzmann's constant, T is the crystallization temperature, ΔG is the thermodynamic driven force (the volumetric free energy difference between melt and crystal), and E_a is the diffusion activation energy across the liquid−nucleus interface. K_n is a constant containing energetic and geometrical factors of the nuclei. $n = 2$ for primary nucleation and $n = 1$ for secondary nucleation.[62]

When flow is imposed, the volumetric free energy of melt is raised and ΔG changes into

$$\Delta G = \Delta G_q + \Delta G_f \tag{4}$$

Here ΔG_q is the thermodynamic driving force at quiescent condition and can be written as

$$\Delta G_q = \Delta H_0\left(1 - \frac{T}{T_m}\right) \tag{5}$$

where ΔH_0 is the latent heat of fusion and T_m is the equilibrium melting point. Furthermore, in eq 4 ΔG_f is the driving force contributed by external field such as the step strain in this work. Note that FIC is a thermodynamically non-equilibrium process, while adding an extra free energy term to account the effect of flow is an approximation of the thermodynamically equilibrium approach,[53,63−65] which has been widely employed in the community though its validity is not fully proven yet.

If ΔG_f can be evaluated, the nucleation rate under flow can be predicted. The Doi−Edwards theory with independent alignment approximation (IAA) was proposed to describe the effect of flow in the linear region. The Hencky strain we used is 1.2, which is small enough to disregard possible chain stretch at high strain rates. The general form given by Marrucci and Grizzuti is written as

$$\Delta G_f = 3ck_BT\int_{-\infty}^{t} \dot{\mu}(t,t')A[\mathbf{E}(t,t')]\,dt' \tag{6}$$

where c is the primitive chain segment concentration, equivalent to the entanglement density. It can be expressed as

$$c = \frac{\rho}{M_e}N_a \tag{7}$$

where ρ is the density of melt, M_e the molecule weight between entanglements, and N_a the Avogadro constant.

The Doi−Edwards memory function $\mu(t,t')$ gives the memory of flow at time t when flow was imposed at time t'. It can be written as

$$\mu(t,t') = \frac{8}{\pi^2}\sum_{p\text{odd}}\frac{1}{p^2}\exp\left[-\frac{(t-t')p^2}{\tau_d}\right] = \frac{8}{\pi^2}Y\left(\frac{t-t'}{\tau_d}\right) \tag{8}$$

where τ_d is the terminal relaxation time and function Y has been substituted for the sum.

The free energy change of a primitive chain segment between times t and t' with $\mathbf{E}(t,t')$ the corresponding deformation tensor is given by $3k_BTA[\mathbf{E}(t,t')]$. We shall refer to $A[\mathbf{E}(t,t')]$ as the free energy change hereafter. Under the condition of uniaxial elongation and shear deformation, $\mathbf{E}(t,t')$ is equivalent to the stretch ratio and shear strain, respectively, when describing the strain state. Hence, $A[\mathbf{E}(t,t')]$ can be rewritten for uniaxial elongation and shear deformation as

$$A[\mathbf{E}(t,t')] = A[\lambda(t,t')] = A[\exp(\int_{z'}^{z} De\,dz'')] \tag{9}$$

$$A[\mathbf{E}(t,t')] = A[\gamma(t,t')] = A(\int_{z'}^{z} De\,dz'') \tag{10}$$

Here $\lambda(t,t')$ and $\gamma(t,t')$ are the elongation ratio and shear strain between t and t'. De is the Deborah number defined as the deformation rate multiplied by the relaxation time. z, z', and z'' are the dimensionless time defined as time divided by the relaxation time.

For uniaxial elongation deformation with an elongation ratio λ we have

$$A(\lambda) = \ln\lambda + \frac{\tan^{-1}(\lambda^3-1)^{1/2}}{(\lambda^3-1)^{1/2}} - 1 \tag{11}$$

and for shear deformation with strain γ we can write

$$A(\gamma) = \frac{1}{2}\int_0^1 \ln\left[\frac{1+\gamma^2x^2+[x^4(\gamma^4+4\gamma^2)-2\gamma^2x^2+1]^{0.5}}{2}\right] dx \quad (12)$$

The above deductions are the result of the microrheological model proposed by Coppola and Grizzuti, which gives a general description of an arbitrary deformation history. While in practice the deformation is mostly imposed in a rather short time, thus eq 6 has to be modified. For a relaxation process with the deformation ceased at time t', the free energy change decays to zero in the following way:

$$A_{\text{relax}}(t) = A[\mathbf{E}(t',-\infty)]\mu(t-t') \quad (13)$$

Making a differential to time $t - t'$, we get the relaxation rate:

$$\dot{A}_{\text{relax}}(t) = A[\mathbf{E}(t',-\infty)]\dot{\mu}(t-t') \quad (14)$$

Note that the relaxation rate is the same independent of whether relaxation or continuous deformation is considered. Hence, the actual free energy change for a continuous deformation up to time t can be calculated by subtracting the contribution of relaxation from that in absence of relaxation:

$$A(t) = A[\mathbf{E}(t,-\infty)] - \int_{-\infty}^{t} A[\mathbf{E}(t',-\infty)]\dot{\mu}(t-t')\,dt' \quad (15)$$

Making the transformation

$$A[\mathbf{E}(t,-\infty)] = \int_{-\infty}^{t} A[\mathbf{E}(t,-\infty)]\dot{\mu}(t-t')\,dt' \quad (16)$$

eq 15 can be written as

$$\begin{aligned} A(t) &= \int_{-\infty}^{t} \{A[\mathbf{E}(t,-\infty)] - A[\mathbf{E}(t',-\infty)]\}\dot{\mu}(t-t')\,dt' \\ &= \int_{-\infty}^{t} A[\mathbf{E}(t,t')]\dot{\mu}(t-t')\,dt' \end{aligned} \quad (17)$$

which is the same as eq 6. When a deformation with finite time is considered, the free energy change can be calculated as

$$A(t) = A[\mathbf{E}(t,0)] - \int_0^t A[\mathbf{E}(t',0)]\dot{\mu}(t-t')\,dt' \quad (18)$$

Further, when considering step strain with a strain rate much higher than τ_d^{-1}, it is a good approximation that no relaxation happens. This is the simplest case to treat and often encounters in experiment. The free energy change at time t after cessation of the deformation at $t = 0$ is the product of the memory function and a constant A_0, which is the free energy change in absence of relaxation:

$$A(t) = A_0\mu(t) \quad (19)$$

Using the expression for $A(t)$, we can estimate the driving force contributed by flow field:

$$\Delta G_f = 3ck_BTA(t) = \frac{24ck_BTA_0}{\pi^2}Y(t) \quad (20)$$

Then the nucleation rate per unit volume can be calculated as

$$\begin{aligned} \dot{N}_{\text{unit}} &= Ck_BT\exp\left(-\frac{E_a}{k_BT}\right)(\Delta G_q + \Delta G_f)\exp\left[-\frac{K_n}{T(\Delta G_q+\Delta G_f)^n}\right] \\ &= C_1[1 + C_2Y(t)]\exp\left\{-\frac{C_3}{[1+C_2Y(t)]^n}\right\} \end{aligned} \quad (21)$$

where

$$C_1 = Ck_BT\exp\left(-\frac{E_a}{k_BT}\right)\Delta G_q,$$
$$C_2 = \frac{24ck_BTA_0}{\Delta G_q\pi^2}, \quad C_3 = \frac{K_n}{T(\Delta G_q)^n} \quad (22)$$

The evolution of the nucleation rate is dominated by the exponential term in eq 21, so the time dependence of the prefactor can be neglected and taken as constant. Now the nucleation rate per unit volume can be expressed as

$$\dot{N}_{\text{unit}}(t) \sim \exp\left\{-\frac{C_3}{[1+C_2Y(t)]^n}\right\} \quad (23)$$

The symbol "∼" means the coefficient is omitted.

II. Calculation of Occupied Volume *V*(*t*) and *L*(*t*). As discussed above, the long period is proportional to the inverse of the nucleation density or alternatively the volume occupied by nuclei divided by the total number of nuclei. The volume can be estimated as follows. Assuming the filling rate holds a linear relation with the unoccupied volume, $V(t)$ can be described as

$$\frac{dV(t)}{dt} = B[V_0 - V(t)] \quad (24)$$

where $V(t)$ is the volume occupied by nuclei and V_0 is the total volume. B is a constant with dimension s^{-1} and reflects the speed of nucleation, which naturally varies between $(0, 1)$. B will be referred to as the volume filling rate hereafter. Solving eq 24, we get

$$V(t) = V_0[1 - \exp(-Bt)] \quad (25)$$

The total nucleation rate depends on the remaining volume hence eq 23 has to be multiplied by $\exp(-Bt)$. Subsequently, the number of nuclei $N(t)$ can be obtained by integration as

$$N(t) \sim \int_0^t \exp\left\{-\frac{C_3}{[1+C_2Y(t')]^n}\right\}\exp(-Bt')\,dt' \quad (26)$$

Combining eq 25 and eq 26, for a given B and τ_d, the long period can be expressed as

$$L(t) = L_0\frac{1-\exp(-Bt)}{\int_0^t \exp\left\{-\frac{C_3}{[1+C_2Y(t')]^n}\right\}\exp(-Bt')\,dt'} \quad (27)$$

where L_0 is a constant.

COMPARISON BETWEEN THEORY AND EXPERIMENT

In this section, we will compare the theoretical model with the long periods obtained from SAXS through numerical fitting. There are six parameters in eq 27, listed as n, L_0, B, C_2, C_3, and τ_d. From these n can be fixed at $n = 2$ for primary nucleation. L_0 is a constant that is determined by the plateau value of the long period. C_2 is proportional to the ratio of the free energy change induced by flow and that in quiescent. Its value can be calculated from eq 22. C_3 depends on surface free energy of the nuclei, which varies with crystallization condition. Though τ_d can be determined by SAOS measurement, the result can only be considered as an estimate of the order of magnitude when a polydispersed sample is used. Thus, we leave three adjustable

dx.doi.org/10.1021/ma201263z |*Macromolecules* 2011, 44, 7704–7712

Table 1. Parameter Combination of Different Strain Rates

strain rate (s^{-1})	τ_d (s)	B (s^{-1})	C_3
100	85	0.24	31
50	100	0.14	26
20	80	0.11	30
10	60	0.06	27

parameters B, C_3, and τ_d for a least-squares fitting of the theory to the experiments.

Before we come to fitting, let us first calculate C_2. Taking ΔH_0 = 266 J/m^3,[66] T_m = 69 °C, and a crystallization temperature T = 58 °C, we obtain $\Delta G_q = 8.56 \times 10^6$ J/m^3. The prefactor of ΔG_f in eq 6 is $3ck_BT = 3\rho RT/M_e = 4.64 \times 10^6$ J/m^3, where R is the gas constant, ρ the density of PEO melt (1.124 g/cm^3), and M_e the molecule weight between entanglement, which is 2000 g/mol for PEO.[67] The Hencky strain 1.2 employed in the current work corresponds to a stretch ratio λ = 3.32. Given that the strain rate is much higher than τ_d^{-1}, which is smaller than 0.1 s^{-1}, the stretch ratio is considered to have the same value of 3.32 for all four strain rates. So A_0 has a value of 0.435. Insertion all these values in eq 22, we arrive at

$$C_2 = \frac{24ck_BTA_0}{\Delta G_q \pi^2} = 0.191 \tag{28}$$

Finally, we simplify the DE memory function of eq 8 by omitting high-order terms in the summation because they decay rapidly with time:

$$\mu(t) = \frac{8}{\pi^2}\sum_{p\text{odd}}\frac{1}{p^2}exp\left(-\frac{tp^2}{\tau_d}\right) = \frac{8}{\pi^2}\left[exp\left(-\frac{t}{\tau_d}\right) + \frac{1}{9}exp\left(-\frac{9t}{\tau_d}\right) + \frac{1}{25}exp\left(-\frac{25t}{\tau_d}\right) + \frac{1}{49}exp\left(-\frac{49t}{\tau_d}\right)\right] \tag{29}$$

With all parameters as discussed above available, a fitting to the experiment was made with the traversal method. The variation range of parameters was set as $10 \le \tau_d \le 100$ s with step 5 s, $0.001 \le B \le 0.5$ s^{-1} with step 0.01, and $20 \le C_3 \le 50$ with step 1. A good agreement with experiment was obtained with the volume filling rate B depending on strain rate while the other two parameters could be taken as approximately constant with τ_d = 81 ± 20 s and C_3 = 28 ± 3. The fitted parameters are listed in Table 1, and the corresponding fitted curves of the long period are presented in Figure 10.

The fitted relaxation time varies between 60 and 100 s, which is in accordance with the measurement of SAOS at higher temperatures. The most relevant variable is the fitting parameter B, which is supposed to reflect the speed of nucleation for different strain rates. In fact, $1/B$ and the induction time of crystallization should correlate positively. We compare the time for the onset of a distinct scattering peak with $1/B$ in Figure 11. Indeed, we find a good agreement in the trend with strain rate. In the fitting, we made the simplification that the free energy change induced by the step strain in the high stain rate region does not vary, which would lead a totally same nucleation behavior. By introducing B the effect of the strain rate is incorporated, which gives an explicit physical meaning to B. This also explains the dominating role of B in fitting.

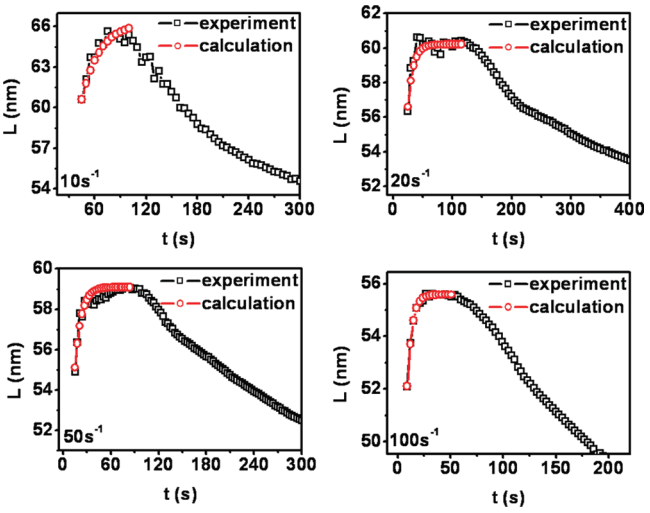

Figure 10. Comparison of calculated and observed long period.

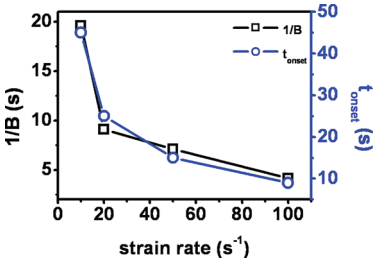

Figure 11. Comparison of $1/B$ and the time for the onset of scattering peak.

C_3 is related to surface free energy of the nuclei. Recalling eq 22, with C_3 = 28 in average and $K_2 = 32\sigma^2\sigma_e/k_B\rho^2$, we get $\sigma^2\sigma_e = 3.70 \times 10^2$ erg^3/cm^6. Taking the surface free energy σ = 10.6 erg/cm^2, σ_e = 22.4 erg/cm^2 obtained at quiescent conditions,[68] we have $\sigma^2\sigma_e = 2.52 \times 10^3$ erg^3/cm^6. Evidently, stretch at high strain rate leads to a sharp drop of the surface free energy, which is in line with the general observation of enhancement of nucleation rate. The decrease in surface free energy can be attributed to a smaller difference in chain conformation between melt and nuclei after deformation.

CONCLUDING REMARKS

The crystallization of PEO induced by extensional flow has been investigated by in-situ SAXS with the emphasis on long period evolution. A monotonic decrease of the long period presents for low strain rates while an initial increase occurs when high strain rates imposed. In order to explain the increase of the long period in high strain rate region, we propose a localized nucleation mechanism. The microrheological model of Coppola et al. used to describe the influence of steady-state flow on nucleation rate has been extended to a step strain for a quantitative description. Taking relaxation of free energy change into account, the nucleation rate decays with nucleation time. The assumption that the volume filling rate B is a constant allows nuclei density to be calculated. The evolution of long period, which is inversely proportional to the nuclei density, has been fitted to our theoretical model, leading to a good agreement. The result confirms the localized nucleation mechanism. It is

supposed to be universal for nucleation in a highly oriented melt. Also, the surface free energy of nuclei induced by flow is lower than that formed at quiescent conditions, which can be understood by a smaller difference in conformation between melt and nuclei after deformation.

Our model is certainly far from consummate. When modeling FIC at molecular level, two grand challenges are confronted, namely nonequilibrium thermodynamic phase transition and nonlinear rheology. (i) FIC of polymer is a process far from thermodynamic equilibrium while up to now no effective approach is established to solve this problem. The thermodynamically nonequilibrium process is a fundamental challenge of condensed matter physics. The thermodynamic equilibrium approach is used as an approximation, and an extra free energy term is commonly added to account the effect of flow. We follow this treatment in our model and some unknown error may be involved, as the validity of this approach still needs to be proven. (ii) The rheological description of the melt under strong flow is still far from mature. It is difficult to describe the rheological behavior in this region even if the inhomogeneity of flow and the polydispersity of polymer are disregarded. At present, we can only deal with the case of a relative small strain or strain rate with some approximations. Additionally, no enthalpy change is considered in our model while the related preordering affects the rheological behavior and phase transition mechanism, which requires detailed structural information on the so-called preordering. Unfortunately, the structures of preordering and even the nucleus are still a puzzle.

AUTHOR INFORMATION

Corresponding Author

*E-mail: lbli@ustc.edu.cn.

ACKNOWLEDGMENT

The authors thank Prof. Wim H de Jeu (Amherst), Prof. Shiqing Wang (Akron), Prof. Masao Doi (Tokyo), Prof. Kaifu Luo (Hefei), and Dr. Bing Miao (Beijing) for fruitful discussions. We are also grateful for advice from Prof. Nino Grittuzi (Naples), especially for the help on our calculation and comprehension about the independent alignment approximation. We acknowledge Prof. Zhigang Wang (Hefei) and Mr. Shiwang Cheng (Akron) for their kindly help on the rheology measurement. We also thank the team in Synchrotron Radiation Facility of Shanghai for supporting during the SAXS measurement. This work is supported by the National Natural Science Foundation of China (51033004, 50973103, 20774091, 20904050), the Fund for One Hundred Talent Scientist of CAS, 973 program of MOST (2010CB934504), Doctoral Fund of MOE (200803580011), and the experimental fund of SSRF and NSRL.

REFERENCES

(1) Janeschitz-Kriegl, H.; Ratajski, E.; Stadlbauer, M. *Rheol. Acta* **2003**, *42*, 355–364.

(2) Kumaraswamy, G.; Kornfield, J. A.; Yeh, F.; Hsiao, B. S. *Macromolecules* **2002**, *35*, 1762–1769.

(3) Hsiao, B. S.; Yang, L.; Somani, R. H.; Avila-Orta, C. A.; Zhu, L. *Phys. Rev. Lett.* **2005**, *94*, 117802.

(4) Seki, M.; Thurman, D. W.; Oberhauser, J. P.; Kornfield, J. A. *Macromolecules* **2002**, *35*, 2583–2594.

(5) Somani, R. H.; Hsiao, B. S.; Nogales, A.; Fruitwala, H.; Srinivas, S.; Tsou, A. H. *Macromolecules* **2001**, *34*, 5902–5909.

(6) Sun, X.; Li, H.; Wang, J.; Yan, S. *Macromolecules* **2006**, *39*, 8720–8726.

(7) Pennings, A. J.; Kiel, A. M. *Kolloid Z. Z. Polym.* **1965**, *20*, 160.

(8) Keller, A.; Machin, M. J. *J. Macromol. Sci., Part B: Phys.* **1967**, *1*, 41–91.

(9) Mackley, M. R.; Keller, A. *Philos. Trans. R. Soc. London* **1975**, *278*, 29–65.

(10) Odell, J. A.; Keller, A.; Muller, A. J. *Polymer* **1985**, *26*, 1219–1226.

(11) Yan, T. Z.; Zhao, B. J.; Cong, Y. H.; Fang, Y. Y.; Cheng, S. W.; Li, L. B.; Pan, G. Q.; Wang, Z. J.; Li, X. H.; Bian, F. G. *Macromolecules* **2010**, *43*, 602–605.

(12) Li, L. B.; Jeu, W. H. *Adv. Polym. Sci.* **2005**, *181*, 75–120.

(13) An, H. N.; Zhao, B. J.; Ma, Z.; Shao, C. G.; Wang, X.; Fang, Y. P.; Li, L. B.; Li, Z. M. *Macromolecules* **2007**, *40*, 4740–4743.

(14) Alfonso, G. C.; Scardigli, P. *Macromol. Symp* **1997**, *118*, 323–328.

(15) Cavallo, D.; Azzurri, F.; Balzano, L.; Funari, S. S.; Alfonso, G. C. *Macromolecules* **2010**, *43*, 9394–9400.

(16) Martins, J. A.; Zhang, W. D.; Brito, A. M. *Polymer* **2010**, *51*, 4185–4194.

(17) Imai, M.; Mori, K.; Mizukami, T.; Kaji, K.; Kanaya, T. *Polymer* **1992**, *33*, 4451–4456.

(18) Imai, M.; Kaji, K.; Kanaya, T. *Phys. Rev. Lett.* **1993**, *71*, 4162–4165.

(19) Olmsted, P. D.; Poon, W. C. K.; McLeish, T. C. B.; Terrill, N. J.; Ryan, A. J. *Phys. Rev. Lett.* **1998**, *81*, 373–376.

(20) Heeley, E. L.; Maidens, A. V.; Olmsted, P. D.; Bras, W.; Dolbnya, I. P.; Fairclough, J. P. A.; Terrill, N. J.; Ryan, A. J. *Macromolecules* **2003**, *36*, 3656–3665.

(21) Zhang, X. H.; Wang, Z. G.; Muthukumar, M.; Han, C. C. *Macromol. Rapid Commun.* **2005**, *26*, 1285–1288.

(22) Gee, R. H.; Lacevic, N.; Fried, L. E. *Nature Mater.* **2006**, *5*, 39–43.

(23) Balzano, L.; Rastogi, S.; Peters, G. W. M. *Macromolecules* **2009**, *42*, 2088–2092.

(24) Hayashi, Y.; Matsuba, G.; Zhao, Y.; Nishida, K.; Kanaya, T. *Polymer* **2009**, *50*, 2095–2103.

(25) Somani, R. H.; Yang, L.; Hsiao, B. S.; Sun, T.; Pogodina, N. V.; Lustiger, A. *Macromolecules* **2005**, *38*, 1244–1255.

(26) Kumaraswamy, G.; Issaian, A. M.; Kornfield, J. A. *Macromolecules* **1999**, *32*, 7537–7547.

(27) Panine, P.; Di Cola, E.; Sztucki, M.; Narayanan, T. *Polymer* **2008**, *49*, 976–680.

(28) Kraack, H.; Deutsch, M.; Sirota, E. B. *Macromolecules* **2000**, *33*, 6174–6184.

(29) Allegra, G.; Meille, S. V. *Adv. Polym. Sci.* **2005**, *191*, 87–135.

(30) Milner, S. T. *Soft Matter* **2011**, *7*, 2909–2917.

(31) Elmoumni, A.; Gonzalez-Ruiz, R. A.; Coughlin, E. B.; Winter, H. H. *Macromol. Chem. Phys.* **2005**, *206*, 125–134.

(32) Heeley, E. L.; Fernyhough, C. M.; Graham, R. S.; Olmsted, P. D.; Inkson, N. J.; Embery, J.; Groves, D. J.; McLeish, T. C. B.; Morgovan, A. C.; Meneau, F.; Bras, W.; Ryan, A. J. *Macromolecules* **2006**, *39*, 5058–5071.

(33) Matsuba, G.; Sakamoto, S.; Ogino, Y.; Nishida, K.; Kanaya, T. *Macromolecules* **2007**, *40*, 7270–7275.

(34) Keum, J. K.; Burger, C.; Hsiao, B. S.; Somani, R. H.; Yang, L.; Chu, B.; Kolb, R.; Chen, H. Y.; Lue, C. T. *Prog. Colloid Polym. Sci.* **2005**, *130*, 114–126.

(35) Hashimoto, T.; Murase, H.; Ohta, Y. *Macromolecules* **2010**, *43*, 6542–6548.

(36) Kimata, S.; Sakurai, T.; Nozue, Y.; Kasahara, T.; Yamaguchi, N.; Karino, T.; Shibayama, M.; Kornfield, J. A. *Science* **2007**, *316*, 1014–1017.

(37) Zhao, B. J.; Li, X. Y.; Huang, Y. J.; Cong, Y. H.; Ma, Z.; Shao, C. G.; An, H. N.; Yan, T. Z.; Li, L. B. *Macromolecules* **2009**, *42*, 1428–1432.

(38) Tapadia, P.; Wang, S. Q. *Phys. Rev. Lett.* **2006**, *96*, 016001.

(39) Tapadia, P.; Wang, S. Q. *Macromolecules* **2004**, *37*, 9083–9095.

(40) Boukany, P. E.; Tapadia, P.; Wang, S. Q. *J. Rheol.* **2006**, *50*, 641–654.

(41) Wang, S. Q.; Ravindranath, S.; Boukany, P.; Olechnowicz, M.; Quirk, R. P.; Halasa, A.; Mays, J. *Phys. Rev. Lett.* **2006**, *97*, 187801.

(42) Fang, Y. Y.; Wang, G. L.; Tian, N.; Wang, X.; Zhu, X. Y.; Lin, P. P.; Ma, G. L.; Li, L. B. *J. Rheol.* **2011**, *55*, 939–949.
(43) Nakamura, K.; Watanabe, K.; Katayama, K.; Amano, T. *J. Appl. Polym. Sci.* **1973**, *17*, 1031–1041.
(44) Ito, H.; Minagawa, K.; Takimoto, J.; Tada, K.; Koyama, K. *Int. Polym. Proc.* **1996**, *11*, 363–368.
(45) Tanner, R. I. *J. Non-Newtonian Fluid Mech.* **2002**, *102*, 397–408.
(46) Doufas, A. K.; McHugh, A. J.; Miller, C. *J. Non-Newtonian Fluid Mech.* **2000**, *92*, 27–66.
(47) Mykhaylyk, O. O.; Chambon, P.; Graham, R. S.; Fairclough, J. P. A.; Olmsted, P. D.; Ryan, A. J. *Macromolecules* **2008**, *41*, 1901–1904.
(48) Mykhaylyk, O. O.; Chambon, P.; Impradice, C.; Fairclough, J. P. A.; Terrill, N. J.; Ryan, A. J. *Macromolecules* **2010**, *43*, 2389–2405.
(49) Kim, K. H.; Isayev, A. I.; Kwon, K. *J. Appl. Polym. Sci.* **2005**, *95*, 502–523.
(50) Zinet, M.; Otmani, R. E.; Boutaous, M.; Chantrenne, P. *Polym. Eng. Sci.* **2010**, *50*, 2044–2059.
(51) Steenbakkersa, R. J. A.; Peters, G. W. M. *J. Rheol.* **2011**, *55*, 401–433.
(52) Bushman, A. C.; Mchugh, A. J. *J. Polym. Sci., Part B: Polym. Phys.* **1996**, *34*, 2393–2407.
(53) Zheng, R.; Kennedy, P. K. *J. Rheol.* **2004**, *48*, 823–842.
(54) Titomanlio, G.; Lamberti, G. *Rheol. Acta* **2004**, *43*, 146–158.
(55) Coppola, S.; Grizzuti, N.; Maffettone, L. P. *Macromolecules* **2001**, *34*, 5030–5036.
(56) Marrucci, G.; Grizzuti, N. *J. Rheol.* **1983**, *27*, 433–450.
(57) Stribeck, N.; Nolchel, U.; Camarillo, A. A.; Roth, S. V.; Dommach, M.; Bolsecke, P. *Macromolecules* **2007**, *40*, 4535–4545.
(58) Talibuddin, S.; Runt, J.; Liu, L. Z.; Chu, B. *Macromolecules* **1998**, *31*, 1627–1634.
(59) Graham, R. S.; Olmsted, P. D. *Phys. Rev. Lett.* **2009**, *103*, 115702.
(60) Graham, R. S.; Olmsted, P. D. *Faraday Discuss.* **2010**, *144*, 71–92.
(61) Lauritzen, J. I.; Hoffman, J. D. *J. Rev. Natl. Bur. Stand.* **1960**, *64A*, 73.
(62) Ziabicki, A. *Colloid Polym. Sci.* **1996**, *274*, 705–716.
(63) Onuki, A. *J. Phys.: Condens. Matter* **1997**, *9*, 6119–6157.
(64) Olmsted, P. D.; Goldbart, P. M. *Phys. Rev. A* **1990**, *41*, 4578–4582.
(65) Olmsted, P. D.; Goldbart, P. M. *Phys. Rev. A* **1992**, *46*, 4966–4993.
(66) Pielichowska, K.; Pielichowski, K. *Thermochim. Acta* **2010**, *510*, 173–184.
(67) Rubinstein, M.; Colby, R. H. *Polymer Physics*; Oxford University Press: New York, 2003; p 371.
(68) Cheng, S. Z. D.; Chen, J. H.; Janimak, J. J. *Polymer* **1990**, *31*, 1018–1024.